

A computational study of the effects of remodelled electrophysiology and mechanics on initiation of ventricular fibrillation in human heart failure

Nathan R Kirk¹, Alan P Benson², Christopher E Goodyer^{1,3}, Matthew E Hubbard^{1*}

1 School of Computing, University of Leeds, Leeds, West Yorkshire, LS2 9JT, United Kingdom

2 School of Biomedical Sciences, University of Leeds, Leeds, West Yorkshire, LS2 9JT, United Kingdom

3 The Numerical Algorithms Group, Wilkinson House, Jordan Hill Road, Oxford, OX2 8DR, United Kingdom

* E-mail: m.e.hubbard@leeds.ac.uk

Abstract

The study of pathological cardiac conditions such as arrhythmias, a major cause of mortality in heart failure, is becoming increasingly informed by computational simulation, numerically modelling the governing equations. This can provide insight where experimental work is constrained by technical limitations and/or ethical issues. It is now commonly used to provide comprehensive studies of the mechanisms underlying the onset of arrhythmias at cell, tissue and organ levels, based on increasingly detailed descriptions of the electrophysiology, derived from experiment.

As the models become more realistic, the construction of efficient and accurate computational models becomes increasingly challenging. In particular, recent developments have started to couple the electrophysiology models with mechanical models in order to investigate the effect of tissue deformation on arrhythmogenesis, thus introducing an element of nonlinearity into the mathematical representation. This paper outlines a biophysically-detailed computational model of coupled electromechanical cardiac activity which uses the finite element method to approximate both electrical and mechanical systems on unstructured, deforming, meshes. An ILU preconditioner is applied to improve performance of the solver.

This software is used to examine the role of electrophysiology, fibrosis and mechanical deformation on the stability of spiral wave dynamics in human ventricular tissue by applying it to models of both healthy and failing tissue. The latter was simulated by modifying (i) cellular electrophysiological properties, to generate an increased action potential duration and altered intracellular calcium handling, and (ii) tissue-level properties, to simulate the gap junction remodelling, fibrosis and increased tissue stiffness seen in heart failure. The resulting numerical experiments suggest that, for the chosen mathematical models of electrophysiology and mechanical response, introducing tissue level fibrosis can have a destabilising effect on the dynamics, while the net effect of the electrophysiological remodelling stabilises the system.

Introduction

Heart failure accounts for over 280000 deaths each year in the United States alone [1], with up to 50% of these deaths being sudden and presumably due to ventricular arrhythmia [2]. Ventricular fibrillation is an often fatal arrhythmia, in which the normal sinus rhythm is disturbed when the same wavefronts continually re-excite the same tissue (re-entry); synchronous contraction of the ventricles is lost, circulation of the blood ceases and death occurs if normal sinus rhythm is not quickly restored [3]. Separately, the sub-cellular, cellular and tissue-level electrophysiological arrhythmia mechanisms underlying heart failure are well studied [2]: common findings include altered calcium handling [4], prolongation of the action potential duration [5], hypertrophy [6], gap junction remodelling [7] and fibrosis [8]. However, it is less

well understood how these different types of remodelling interact at the tissue and organ levels to induce arrhythmias.

The study of cardiac arrhythmias has been a major focus of computational biology, as a detailed quantitative description of the underlying electrophysiology has been developed that allows the simulation of both normal and pathological excitation and propagation of this excitation [9, 10]. As experimental studies of cardiac arrhythmias at the tissue and organ levels have been largely limited to voltage recordings on or near the surface of a preparation [11, 12], computational models offer an additional research tool that can enhance results from experimental studies [13] or can give insights into the functioning of the heart that cannot be gained through experimental work, either due to technical limitations or ethical issues [14]. The results of such simulations can be dissected in time and space, and investigated over a broad range of parameter values, allowing a detailed study at the cell, tissue and organ levels of the mechanisms underlying the onset of arrhythmias [15], and interventions aimed at either preventing this onset [16, 17] or restoring normal sinus rhythm [18, 19].

Recently, these electrophysiology models have been coupled to mechanical models in deforming domains in order to investigate the additional influence that mechanics has on arrhythmogenesis [20–22]. For example, [20] showed that breakdown of a re-entrant wave into a chaotic state (*i.e.* the transition from ventricular tachycardia to fibrillation) occurred later in a contracting compared to a non-contracting domain. However, these studies often use either phenomenological models that, due to their simplicity, limit the application of the model to a disease state (*e.g.* [20]), or use biophysically-detailed (and therefore computationally-demanding) models that make longer simulations intractable without access to high-performance computing facilities (*e.g.* [21]). An efficient, biophysically-detailed, electromechanical model is therefore a useful research tool.

The aims of this study were: (i) to develop a biophysically-detailed, coupled electromechanical model of human tissue that could be used to study re-entrant arrhythmias in both healthy and failing states; (ii) to tailor this model to reproduce the cell- and tissue-level remodelling observed with heart failure; and (iii) use the modified model to examine the roles of electrophysiology (ionic currents, calcium handling, gap junctions), fibrosis and mechanical deformation on the initiation of ventricular fibrillation in heart failure.

In this paper the biophysically-detailed human electrophysiology model of ten Tusscher and Panfilov [23] is coupled with a Mooney-Rivlin mechanical model of elastic material (as in [20]), leading to two systems of partial differential equations which are approximated on unstructured, triangular meshes in two space dimensions using the finite element method. First, the electrophysiology and mechanics models are outlined, followed by a description of the modifications required to distinguish failing from healthy tissue. Next, the computational model used to approximate this system is described briefly and its behaviour illustrated by applying it to healthy/control versions of the electrophysiology and mechanics systems. This is then used for the subsequent investigation of the roles of remodelled electrophysiology, fibrotic tissue and mechanical deformation on spiral wave dynamics in human ventricular tissue, a key indicator in many dangerous cardiac arrhythmias [24].

Methods

To simulate coupled cardiac electromechanical activity it is necessary to model the propagation of the electrical waves around the heart muscle, the muscle contraction instigated by this electrical activity and the feedback that the electrical activity and muscle deformation have upon each other. This section will provide an outline of the mathematical models used to represent the coupled electromechanical activity, the computational algorithms which were used to approximate this mathematical system, and the meshes on which the computations were carried out.

Electrophysiology Model

For this study, a monodomain model was used to represent cardiac electrophysiology, as described by [25]

$$\frac{\partial V}{\partial t} = -(I_{\text{ion}} + I_{\text{stim}}) + \nabla \cdot (\mathbf{D}\nabla V), \quad (1)$$

where \mathbf{D} is the diffusion tensor, V is the transmembrane potential, I_{ion} is the sum of all ionic currents, and I_{stim} is the externally applied transmembrane current. On the boundary of the domain, zero flux conditions are imposed, *i.e.* $\nabla V \cdot n = 0$, where n is the outward pointing normal to the boundary. The detailed description of the ionic currents I_{ion} was provided by the ten Tusscher and Panfilov 2006 model (referred to hereafter as TP06) [23], which presents a detailed description of individual ionic currents and intracellular ion concentrations in human epicardial ventricular cells. This is a biophysically-detailed model, based on human electrophysiological data, and provides the potential to simulate the conditions of end-stage tissue failure examined later in this paper.

Mechanics Model

The cardiac tissue was modelled as a nonlinearly elastic material. The governing stress equilibrium equations [20] take the general form

$$\frac{\partial}{\partial X_M} (T^{MN} F_N^j) = 0, \quad (2)$$

where T^{MN} is the second Piola-Kirchhoff stress tensor and \mathbf{F} is the deformation gradient tensor,

$$F_N^j = \frac{\partial x_j}{\partial X_N}. \quad (3)$$

The unknown variables x_j represent the deformed coordinate system, while X_N are the reference coordinates, relative to which the deformed coordinates are defined. The indices M, N, j represent the coordinate axes and take the values $1, \dots, d$, where d is the number of space dimensions. These equations are derived from conservation of linear momentum, following Newton's laws of motion [26], and their solution provides the material deformation. In common with other authors [27, 28] the tissue is assumed to be incompressible, a constraint which is enforced by imposing

$$\det(\mathbf{F}) = 1, \quad (4)$$

as in [22]. On the boundary of the domain a zero normal stress is imposed.

In common with [22], the second Piola-Kirchhoff tensor is split into an elastic component and a biochemical component, giving

$$T^{MN} = \underbrace{\frac{1}{2} \left(\frac{\partial W}{\partial E_{MN}} + \frac{\partial W}{\partial E_{NM}} \right)}_{\text{elastic}} - p C_{MN}^{-1} + \underbrace{T_a C_{MN}^{-1}}_{\text{biochemical}}, \quad (5)$$

where W is the scalar strain energy function, $\mathbf{E} = \frac{1}{2}(\mathbf{C} - \mathbf{I})$ is the Lagrange-Green strain tensor ($\mathbf{C} = \mathbf{F}^T \mathbf{F}$ being Green's strain tensor), p is a Lagrange multiplier that is used to enforce the incompressibility constraint (4) and is an additional unknown variable commonly referred to as the pressure, and T_a is the active tension generated by the electrophysiology. Following [20], the strain energy function for Mooney-Rivlin materials [29, 30] is used. This is given by

$$W(I_1, I_2) = c_1(I_1 - 3) + c_2(I_2 - 3), \quad (6)$$

where $I_1 = \text{tr } \mathbf{C}$ and $I_2 = \frac{1}{2}[(\text{tr } \mathbf{C})^2 - \text{tr } \mathbf{C}^2]$ are the first and second invariants of the Cauchy-Green deformation tensor (tr being the trace of the tensor \mathbf{C} , the sum of its diagonal elements). Throughout this work, the parameters c_1 and c_2 were set to 2 kPa and 6 kPa, respectively. It has been shown experimentally that cardiac tissue exhibits different responses along the various material axes [31] so, since the chosen strain energy function is isotropic, the biochemical component in Equation (5) is set so that the active tension acts in only one direction, coinciding with the major axis of the diffusion tensor \mathbf{D} , as described in [22]. This ensures that the forces generated by the biochemical activity act along the direction of fibre orientation [28, 32].

The last component of Equation (5) governs the response of the mechanics to the active tension (T_a) generated by the biochemical activity in the tissue. In [20] (Equations (22c) and (23), subsequently updated at www.cellml.org), a phenomenological description of the tension within cardiac tissue is provided, in which the active tension is determined by the transmembrane voltage, *i.e.* we use

$$\frac{dT_a}{dt} = \epsilon(V_t)(K_{T_a}V_t - T_a), \quad (7)$$

where $K_{T_a} = 9.58$ kPa is a parameter which controls the maximum amplitude of the active tension (T_a), V_t is the normalised transmembrane voltage (scaled linearly so that $0 \leq V_t \leq 1$), and

$$\epsilon(V_t) = \begin{cases} 10\epsilon_0 & \text{for } V_t < 0.005 \\ \epsilon_0 & \text{for } V_t \geq 0.005. \end{cases} \quad (8)$$

The value of ϵ_0 was taken to be 1. Note that in [33] (see Section 7.3) the active tension was determined by the calcium transient instead of the transmembrane voltage. This has a much steeper wave descent which slightly reduces the overall tissue deformation. However, it did not change the conclusions that could be drawn about the effects of tissue remodelling on spiral wave stability.

Simulating Heart Failure

Electrophysiological arrhythmia mechanisms underlying cardiac disease are well studied [2], with common findings including altered calcium handling [4] and prolongation of the action potential duration [5]. To simulate failing tissue, some components of the ionic currents, I_{ion} in Equation (1), were amended from those presented in the original ten Tusscher and Panfilov model [23]: the transient outward current (I_{to}) maximal conductance was reduced by 48% [34], the inward rectifier potassium current (I_{K1}) was reduced by 44% [35], the sodium-potassium pump current (I_{NaK}) was reduced by 40% [36], the sodium-calcium exchanger current (I_{NaCa}) was increased by 80% [37] and sarcoplasmic reticulum uptake current (I_{up}) reduced by 30% [38, 39]. These changes, referred to from now on as the remodelled electrophysiology, are designed to simulate failing tissue by increasing the resting membrane potential and prolonging duration.

In heart failure, gap junctions (that allow current flow between cells) are reorganised, and instead of being principally located at the ends of the cells, they become “lateralised” so that there is an increase in transverse gap junction numbers and a decrease in longitudinal gap junction numbers within a single cell. However, because of the changes in cell size with the hypertrophy that accompanies heart failure, there is no net change in gap junction numbers in the transverse direction, but still a net decrease (of between 28% [40] and 40% [41]) in longitudinal gap junction numbers [42]. Gap junction changes will affect cell resistivity but, because the electrophysiology model, Equation (1), treats the tissue as a continuum, this resistivity is made up of a “myoplasmic resistivity” (caused by the structures inside the cell) and a “junctional resistivity” (caused by the gap junctions between cells). We assume that junctional resistivity accounts for 22% of total resistivity [43] and that a reduced gap junction expression (33% for our simulations) is followed by a corresponding increase in junctional resistivity [43]. Thus, the cumulative effects of gap junction remodelling is introduced simply by modifying the diffusion tensor in Equation (1). Diffusion in control tissue was set to $0.154 \text{ cm}^2/\text{ms}$ along the fibre axis, and reduced

nine-fold (to reduce conduction velocity three-fold) in the cross-fibre direction. In heart failure, diffusion in the fibre direction was reduced to $0.139 \text{ cm}^2/\text{ms}$, with cross-fibre diffusion remaining at its control level.

Fibrotic tissue within the cardiac muscle contributes to an increase in the incidence of atrial and ventricular arrhythmias [44, 45]. Exactly how the fibrosis contributes to the generation of arrhythmias is unknown, but impaired electrical conduction is a significant contributory factor [46, 47]. In the normal healthy heart, approximately 6% of cardiac muscle is made from extra-cellular connective tissue [46, 48]. However, in a diseased heart, there is increased formation of fibrotic cells which increases the percentage of connective tissue to between 10% and 35% [46, 48]. To simulate the effects of diffuse fibrosis a large number of small areas within the domain were set to be inexcitable, as in [46]. In these simulations approximately 27% of the tissue was designated inexcitable, within the range seen experimentally [46, 48]. These areas remain in the mechanics system, but do not contract due to the electrical wave since they are inexcitable. Hence they have no electrically-activated tension and do not contribute to the active tissue deformation, instead maintaining their passive deformation properties.

Computational Methods

This section provides a brief outline of the computational algorithms chosen and further details of their implementation for this particular application can be found in [33]. Both the electrophysiology and the mechanics were approximated on unstructured triangular meshes using the finite element method (FEM). Although the computational domains used in this work were all rectangular, the use of unstructured triangles provides flexibility for future simulations on the complex geometries required for realistic representation of a whole ventricle or a complete heart. Furthermore, the use of unstructured meshes avoids the systematic introduction of mesh-induced anisotropy, as illustrated by the mild squaring of the wave-fronts visible in the numerical results presented in [23], a phenomenon which is exaggerated by the steepness of the wave-fronts generated by the TP06 model.

The time-dependent equation governing the electrophysiology, Equation (1), was discretised using the Galerkin FEM. The spatial variation of the unknown variable (V) was represented by a continuous, piecewise linear, function (providing second order accuracy in space) where the unknowns of the discrete system are the values of this function at the nodes of the triangular mesh [49]. The temporal variation of these discrete nodal values was approximated using a semi-implicit approach in which the Crank-Nicolson method was applied to the diffusion term (for which it is unconditionally stable, so the time-step can be chosen independently of the prohibitive stability restrictions imposed on explicit schemes when the spatial mesh is refined, and second order accurate [50]) and the reaction term was approximated using an explicit forward Euler method. The sparse system of linear equations resulting from the implicit FEM approximation was solved using an ILU-preconditioned GMRES solver [51], as implemented in the SPARSKIT software (www-users.cs.umn.edu/~saad/software/SPARSKIT/). The forward Euler method was also applied to the evolution of the active tension, Equation (7).

After a specified number of time-steps (10 in this work) of the electrophysiology system, the updated active tension was used to produce a new estimate of the deformation of the tissue via the stress equilibrium equations, (2) coupled with (4). These were also approximated using the FEM on an unstructured triangular mesh, though the nature of this mathematical system necessitated a slightly different approach. The unknown deformed coordinate system (defined by x_j , $j = 1, 2$) was represented by a pair of continuous, piecewise quadratic, functions where the unknowns of the discrete system are the values of these functions at both the nodes and the edge-midpoints of the triangular mesh, but the unknown pressure variable (p) was, like V , approximated by a continuous, piecewise linear, function with the unknown values at the mesh nodes. This additional level of complexity in the representation is required to produce a stable algorithm [49]. The resulting, highly nonlinear, discrete system was solved with a matrix-free Newton-Krylov iterative method [52], in which the GMRES algorithm [51] was used to solve the linear system which occurs at each iteration of the Newton method for solving the nonlinear system. The initial

estimate required by the Newton method was provided by linear extrapolation from the two previously calculated sets of discrete deformed coordinates. The efficiency of the mechanics solver was significantly enhanced by applying an ILUT preconditioner [53, 54]. This typically improved performance by a factor of more than 20 [33]. We note though that, while this is a significant improvement, the approach is not optimal, and that in the future more sophisticated preconditioners, based on the multigrid approach, have the potential to provide iterative convergence rates that are independent of the system size. To prevent spurious rotation and translation, and hence preserve uniqueness of the numerical approximation of the tissue deformation, the mesh node closest to the centre of the domain was fixed in space and a neighbouring node selected to be at the same vertical height, was not allowed to move in the vertical direction [33].

In order to resolve the steep wave fronts which occur within the electrical waves produced by the TP06 model and, consequently, to produce a numerically-converged approximation of the wave speed, it was necessary to approximate the electrophysiology system on a fine mesh [23, 33]. In contrast, the variations in the tissue deformation are much smoother, so the mechanics system does not need to be approximated on such a fine mesh to produce numerically converged results [22, 33]. This is fortuitous because it is the solution of the discrete mechanics system which is the bottleneck in the computation: if the same computational mesh is used it typically takes 100s-1000s times longer to solve the mechanics system than the electrophysiology system, even with preconditioning enabled [33]. Therefore, the electrophysiology and mechanics systems were solved on two different meshes and, in order to simplify the communication between the two numerical solvers, the electrophysiology mesh was derived by repeated uniform refinement of the mechanics mesh, *i.e.* one mesh is embedded within the other so no interpolation is required to couple the two components, although the active tension (T_a) must be integrated over multiple elements of the electrophysiology mesh in order to evaluate it on the mechanics mesh when approximating Equations (2) and (5).

The electrophysiology and gap junction remodelling were both introduced into the computational model by changing the appropriate physiological parameters. The fibrotic tissue manifests itself as many small regions of non-conduction within the electrophysiology model, which were represented by removing patches of computational elements from the electrophysiology meshes, and applying Neumann no-flux conditions at the boundaries of these patches [46]. The positions of the patches were chosen randomly, though care was taken to ensure that they were separated by at least one layer of mesh elements. No modification to the mechanics mesh was necessary since these patches simply provide zero contribution to the active tension which determines the local tissue deformation.

The combination of using (i) a coarse mechanics mesh embedded in a finer electrophysiology mesh, (ii) implicit time-stepping for the diffusion terms, (iii) multiple time-steps of the electrophysiology between updates of the mechanical deformation, and (iv) ILU preconditioning for both electrophysiology and mechanics systems, massively reduced the CPU time required to undertake these simulations. With this approach, our solver is efficient enough that the simulations of re-entry presented in this paper remained tractable on a desktop PC (Intel Xeon E5420, 2.5 gigahertz clock speed, 4 gigabytes memory).

Results

The results presented in this section are chosen to illustrate the effects on the stability of two-dimensional spiral waves, on both static and deforming domains, of: (i) remodelled electrophysiology; (ii) gap junction remodelling and fibrosis; and (iii) a combination of both.

Test Cases and Initialisation

The simulations were performed on unstructured triangular meshes covering a 120 mm \times 120 mm square domain. In all cases an initial, stable, spiral wave was generated by first applying a 52 mV stimulus for

1 ms to the left face of the domain (using I_{stim} in Equation (1)) to initiate a planar wave-front propagating perpendicular to that face. As this wave traverses the middle of the domain (at 115 ms), the voltage in the whole of the lower half of the domain was overwritten and fixed to the resting potential for a short period of time (35 ms in this case), after which a spiral wave evolves around the end of the wave-front which has been created in the centre of the domain. The simulation was continued for 5000 ms to ensure that the spiral wave dynamics had settled down to a regular periodic behaviour. This was carried out with the parameters of the TP06 model of electrophysiology in healthy tissue [23] chosen to simulate a restitution slope of 1.1, providing stable spiral wave structures with which to initialise all of the simulations presented in this paper. Separate initialising computations were needed for each different computational mesh used and computations which included electromechanical coupling were initialised on deforming domains. This allowed investigation of whether or not the modified conditions (deformation, remodelling, fibrosis) would destabilise an initially stable spiral wave structure. For the simulations involving fibrosis the regions of non-conducting tissue, introduced by removing patches of elements from the computational mesh, were present during the initialisation as well as the subsequent simulation.

Electrophysiology

In order to provide a set of control results with which later simulations can be compared, simulations on a static domain were carried out with electrophysiology represented by the TP06 model [23] and an anisotropic diffusion tensor providing a diffusion rate of $0.154 \text{ cm}^2/\text{ms}$ along the fibre axis, acting diagonally from bottom-left to top-right across the domain, and reduced nine-fold in the cross-fibre direction. The unstructured triangular mesh used (made up of 634368 triangles and 318065 nodes) had an approximate average edge-length of 0.21 mm. This is comparable to the regular finite difference mesh used in [55], in which the nodes were a distance 0.2 mm apart. The time-stepping for the approximation to Equation (1) was carried out with a fixed time-step of 0.08 ms. The mesh on which the tissue deformation was approximated in the following computations was considerably coarser (with only 2478 triangles, equating to 11429 degrees of freedom).

Simulations were undertaken using dynamic restitution slopes of 1.1, 1.4 and 1.8 (as defined in Table 2 of [23]). The changes in the restitution slope alter the action potential profile: the higher-valued slopes correspond to increased resting potentials, higher plateaux and prolonged duration, as can be seen by comparing the panels of Figure 1. Snapshots of the results of these simulations, shown in Figure 2, demonstrate qualitatively similar behaviour to that seen in Figure 7 of [23]. In particular, with their “standard” I_{Na} dynamics (the first column of that figure), the initially stable spiral wave is maintained with restitution slopes of 1.1 and 1.4, but with a restitution slope of 1.8 the spiral wave breaks up into a chaotic state. For a restitution slope of 1.4, panels **C** and **D** of Figure 2 show that small perturbations to the voltage profile, due to the transition from an initial state derived from a spiral wave produced using a restitution slope of 1.1, are still visible after 1000 ms, but have been smoothed out by the time the simulation has reached 3000 ms. The spiral wave becomes progressively less stable as the restitution slope increases.

The effect of coupling the electrophysiology and mechanics components of the model was investigated in [56], which presented the results obtained by repeating these numerical experiments on a deforming domain. The snapshots presented in Figure 3 of that paper are indicative of the tendency for the inclusion of mechanical response and tissue deformation (in the case where the TP06 electrophysiology model is coupled with the Mooney-Rivlin mechanical model) to destabilise spiral waves: for a dynamic restitution slope of 1.4 the spiral wave which is stable in a static domain is unstable in a deforming domain.

Remodelled Electrophysiology

Figure 3 illustrates the effect that remodelling the electrophysiology to represent failing tissue has on spiral wave dynamics. The snapshots shown focus on the simulation with restitution slope 1.8, since this

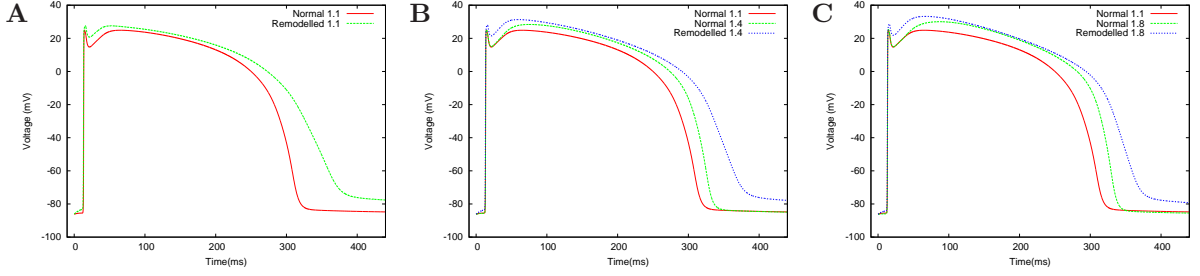


Figure 1. Effect of restitution slope on transmembrane voltage. Comparison of transmembrane voltage profiles for the TP06 model, sampled at a single node of the unstructured computational mesh, for normal and remodelled electrophysiology: (A) restitution slope of 1.1; (B) restitution slope of 1.4; (C) restitution slope of 1.8.

Mesh	N0	F0	F1	F2	F3
Patch Area	N/A	8.72 mm ²	1.93 mm ²	0.53 mm ²	0.27 mm ²
Spiral Wave Stability	Stable	Unstable	Unstable	Unstable	Stable

Table 1. The computational domains used for the fibrosis simulations to investigate the effect of varying the individual patch size. The first column contains the mesh used for simulating normal tissue, *i.e.* without fibrotic regions. The subsequent columns describe meshes in which the size of the individual fibrotic regions (patch area) is varied. In each case the number of fibrotic regions is chosen so that approximately 27% of the mesh area is removed randomly to represent the non-conducting fibrotic areas. The final row indicates the stability of a spiral wave in a static domain when the restitution slope is 1.4. All meshes produced an unstable spiral wave in a deforming domain.

is the only one in which the stability of the spiral wave has been visibly altered. In this case a spiral wave which clearly broke up in the control tissue, on both static and deforming domains, remains stable when the remodelled electrophysiology was introduced. The remodelling also stabilised the spiral wave when it was modelled on a static domain (results not shown here). When the restitution slope was fixed at 1.1 or 1.4 the spiral wave was already stable in the control tissue and this stability was not disturbed by the remodelling.

Gap Junction Remodelling and Fibrosis

The effects of changes in tissue properties, represented by the introduction of gap junction remodelling and regions of non-conducting tissue, in the absence of electrophysiology remodelling were investigated using a series of cases, summarised in Tables 1 and 2, in which the parameters relating to the size and distribution of the patches of inexcitable tissue, introduced to represent diffuse fibrosis, were varied. Both tables show stability on static domains: all situations were unstable when the analogous simulations were carried out on deforming domains.

Initially, spiral wave stability was investigated on static domains, and the size of each patch of fibrotic tissue was varied, as described in Table 1. In all cases, approximately 27% of the tissue was designated as inexcitable in total.

Figure 4 shows that, in the case where a restitution slope of 1.4 was used with mesh F0 (see Table 1), the mesh with the largest fibrotic regions, the introduction of the remodelled tissue has caused an otherwise stable spiral wave to break up. The spiral wave behaviour for the other restitution slopes

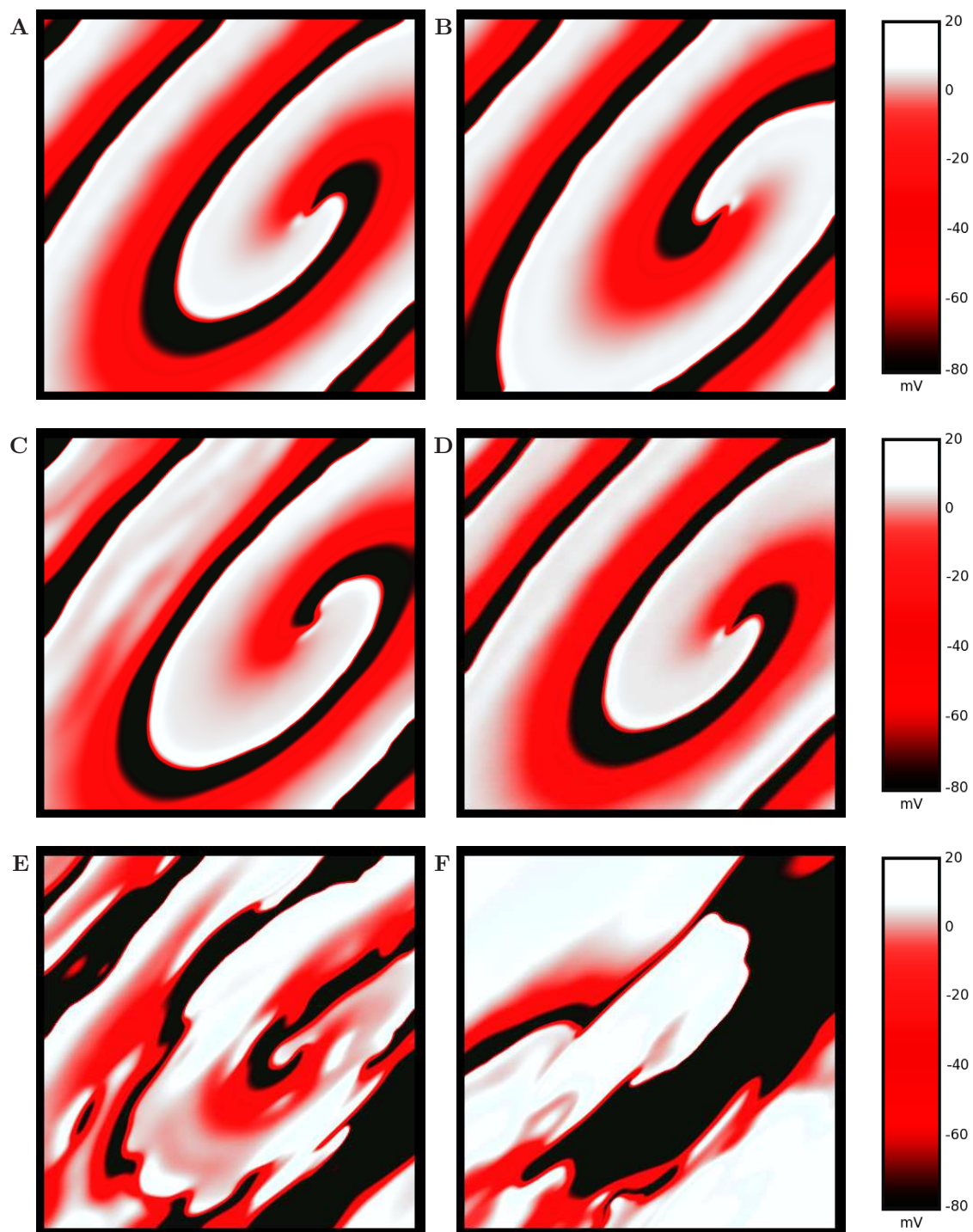


Figure 2. Control experiments. Snapshots of spiral wave dynamics for control tissue without deformation. Each row illustrates the voltage at $t = 1000$ ms (left) and $t = 3000$ ms (right). Results are shown for restitution slopes of 1.1 (A, B), 1.4 (C, D) and 1.8 (E, F).

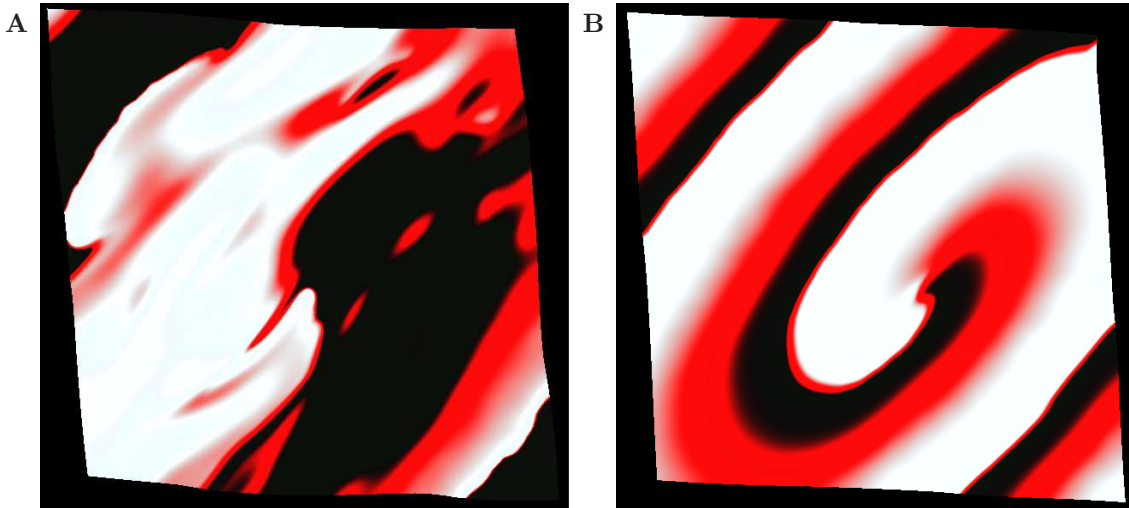


Figure 3. Effects of remodelled electrophysiology. Snapshots of spiral wave dynamics for a deforming domain with a restitution slope of 1.8, taken at $t = 7000$ ms with (A) control electrophysiology and (B) remodelled electrophysiology.

Mesh	F1	F5	F6	F7	F8
Inexcitable Region	26.81%	24.81%	20.17%	15.39%	5.09%
Spiral Wave Stability	Unstable	Unstable	Unstable	Unstable	Unstable

Table 2. The computational domains used for the fibrosis simulations investigating the effects of varying the total proportion of fibrotic tissue. The columns describe meshes in which the proportion of the domain designated as fibrotic (and hence non-conducting) is varied. In each case the average area of the individual fibrotic regions is chosen to be 1.93 mm^2 , as in mesh F1, repeated from Table 1. The final row indicates the stability of a spiral wave in a static domain when the restitution slope is 1.4. All meshes produced an unstable spiral wave in a deforming domain.

tested was not visibly affected: in particular, the effect was not strong enough to destabilise the system when the restitution slope is 1.1. For this reason, only the results obtained with a restitution slope of 1.4 have been investigated further in this section. The results obtained when the domain was allowed to deform are also not shown, since the mechanical deformation has a further destabilising influence but not one strong enough to change the dynamics significantly when the restitution slope was 1.1. The results presented in Figure 5 and summarised in the final row of Table 1 indicate that, as the individual fibrotic regions become smaller, their destabilising effect is progressively reduced.

Next, the average area of the individual fibrotic regions was fixed at 1.93 mm^2 (mesh F1) and the proportion of the total tissue area designated as fibrotic was varied, as indicated in Table 2. The range of fibrotic tissue density is kept within the bounds seen in real tissue [46,48]. It can be seen in Figure 6 that, even with smaller proportions of the domain designated as inexcitable, the spiral wave is still destabilised. Furthermore, there is no clear dependence of the time taken to the start of the spiral wave break-up on the proportion of fibrotic tissue. Even a small number of fibrotic patches can have a significant impact on spiral wave stability: for example, in panel D of Figure 6 a smaller spiral wave is visible in the top-left corner of the domain which has split from the main wave.

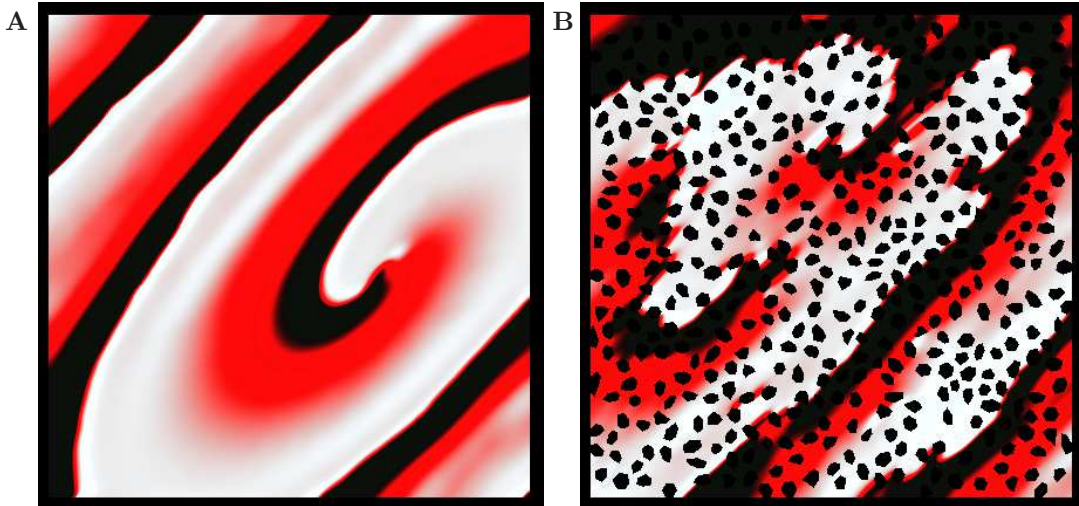


Figure 4. Effects of diffuse fibrosis. Snapshots of spiral wave dynamics for (A) control tissue and (B) remodelled tissue (gap junctions, fibrosis) with a restitution slope of 1.4, taken at $t = 5000$ ms on a static domain. The patches of fibrotic tissue are clearly visible in the right hand panel and have an average area of 8.72 mm^2 (mesh F0 of Table 1).

Combining Electrophysiology and Tissue Remodelling

Finally, all of the proposed enhancements and modifications were included, *i.e.* coupled electromechanics on a deforming domain, remodelled electrophysiology, gap junction remodelling and regions of inexcitable fibrotic tissue. Snapshots of the behaviour for a typical run are shown in Figure 7. Panel B shows that in this case the spiral wave remains stable for a restitution slope of 1.8. The combination of the restitution slope of 1.8 and the deforming domain is the least stable configuration considered in this work: all other combinations tested remained stable.

Discussion

In this paper, a computational model of coupled cardiac electromechanical activity was described and used to investigate the effect on spiral wave stability of changes in cardiac electrophysiology and tissue mechanics manifest in end-stage heart failure. The electrophysiology was represented by the second-generation cellular model proposed by ten Tusscher and Panfilov [23] combined with anisotropic diffusion, the latter providing more rapid diffusion along the fibre direction. The mechanical properties were based on those of an incompressible Mooney-Rivlin material [29,30] in which, to simulate anisotropy, the active tension acted only along the fibre direction. The active tension, which governs the mechanical response to the electrical dynamics, was estimated using a phenomenological dependence on voltage [20]. Analogous experiments have been carried out [33] in which the active tension was instead chosen to depend on the local calcium concentration, but this led to the same conclusions about the stabilising and destabilising effects of the remodelling and mechanical feedback.

The finite element method was used to approximate both the electrophysiology and mechanics models on unstructured triangular meshes, offering the flexibility to model geometrically complex domains in the future. For both systems, numerical methods were chosen for the spatial discretisation which did not require artificial stabilisation techniques. A semi-implicit time-stepping scheme was used for the electrophysiology to ensure that the length of the time-step allowed by stability constraints on the com-

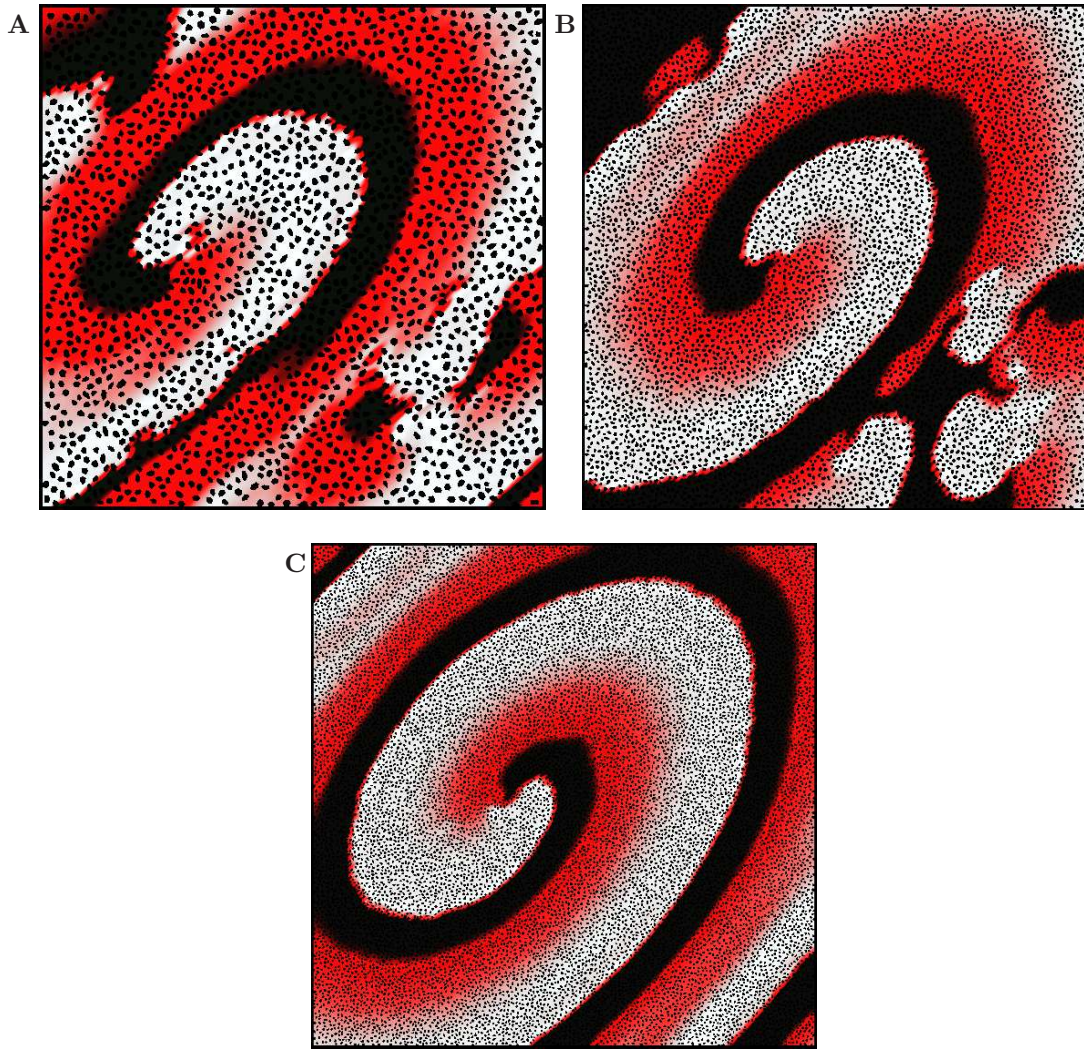


Figure 5. Effects of varying fibrotic patch size. Snapshots of spiral wave dynamics for remodelled tissue (gap junctions, fibrosis) with a restitution slope of 1.4 on a static domain, sampled at **(A)** $t = 13600$ ms on mesh F1, **(B)** $t = 12360$ ms on mesh F2 and **(C)** $t = 17400$ ms on mesh F3 (all meshes from Table 1). In each case the fibrotic tissue constitutes approximately 27% of the total domain area. The times for the snapshots are chosen to indicate the time that break-up first becomes clearly visible or, if break-up does not occur, the end-time of the numerical simulation.

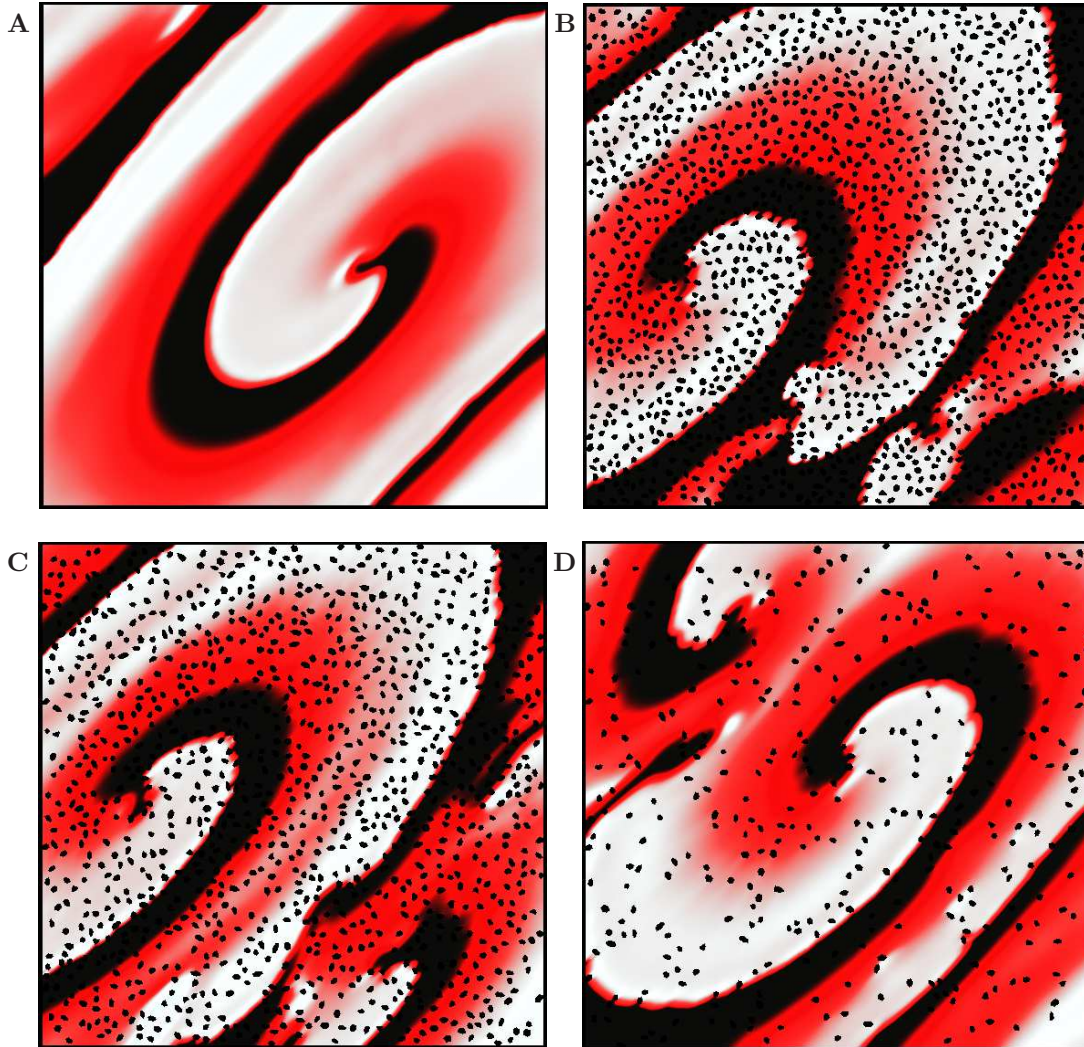


Figure 6. Effect of varying fibrotic patch density. Snapshots of spiral wave dynamics for remodelled tissue (gap junctions, fibrosis) with a restitution slope of 1.4 on a static domain, sampled at (A) $t = 10720$ ms on the control mesh N0, (B) $t = 8600$ ms on mesh F6, (C) $t = 8200$ ms on mesh F7 and (D) $t = 10720$ ms on mesh F8 (all meshes from Table 2). In each case the individual fibrotic regions are, on average, approximately 1.93 mm^2 in area. The times for the snapshots are chosen to indicate the time that break-up first becomes clearly visible or, if break-up does not occur, the end-time of the numerical simulation.

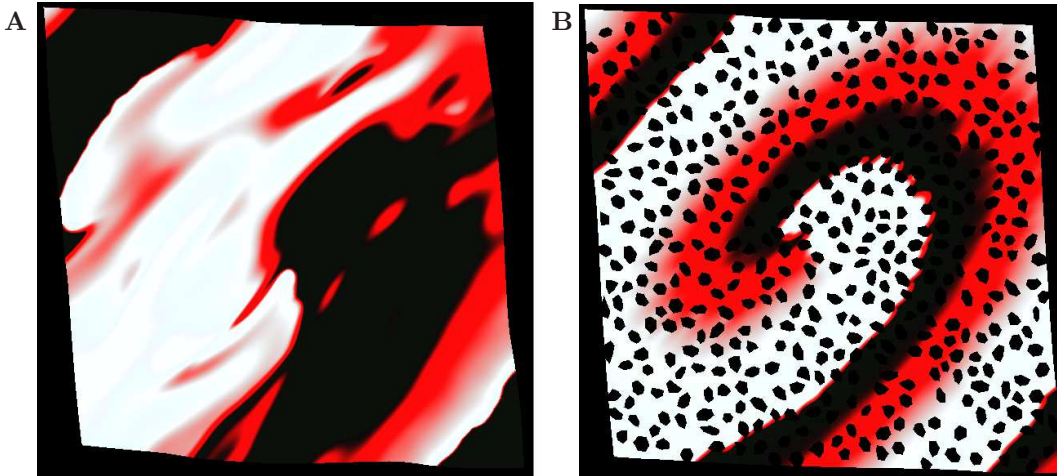


Figure 7. Effect of full electrophysiology and tissue remodelling. Snapshots of spiral wave dynamics for (A) control tissue on mesh N0 and (B) remodelled electrophysiology and tissue (gap junctions, fibrosis) on mesh F0, with a restitution slope of 1.8, taken at $t = 7000$ ms on a static domain.

putation was not limited (via the diffusion term) by the resolution of the spatial mesh. The nature of the mathematical models and their subsequent discretisation dictates that not only is the discrete mechanics system about five times the size of the discrete electrophysiological system if approximated on the same computational mesh, it is also highly nonlinear – therefore it is the solution of the discrete mechanics system that dominates the computation time. However, since the mechanical behaviour acts over longer length scales than the electrical behaviour it does not need such a fine computational mesh to resolve the dynamics so, in this work, the mechanics system was discretised on a much coarser mesh. Interpolation between meshes was avoided by defining the mesh on which the electrophysiology system was discretised to be a uniform refinement of that on which the mechanics system was discretised.

The efficiency of the computational algorithm was improved by the application of an ILU preconditioner [53,54] to the linear systems of equations which need to be solved for each implicit time-step in the electrophysiology system and at each iteration of the Newton solver applied to the nonlinear mechanics system. This is a general-purpose preconditioner which, by careful choice of the algorithm parameters, typically improved the computational performance by a factor of about 20. Preliminary results, presented in [33] but not shown here, suggest that the efficiency could be further improved with the aid of adaptive mesh refinement. Furthermore, this preconditioner is not optimal, and there is the potential to construct a multigrid-based preconditioner for which the number of iterations required to reach convergence is independent of the problem size (and hence the mesh resolution).

The spiral wave dynamics were investigated by studying three test cases, distinguished by sets of conductance parameter values chosen to give different dynamic restitution slopes (1.1, 1.4, 1.8) demonstrating progressively less stable dynamics [23]. With the chosen parameters the spiral wave generated by the TP06 model *without* mechanical deformation is stable for restitution slopes of 1.1 and 1.4 but unstable for a restitution slope of 1.8. When mechanical deformation is included the spiral wave becomes unstable for a restitution slope of 1.4 (but remains stable for 1.1), as indicated in Table 3. This supports the findings in [20,56], that including mechanical response and feedback can reduce the stability of a spiral wave.

Both the electrophysiology and tissue models were modified to imitate the effects of end-stage heart failure. It was seen that electrophysiology remodelling alone, achieved simply by modifying the parameters in the TP06 model [23], can have a stabilising effect on spiral wave dynamics (see Figure 3 and Table

Static Tissue			
	Restitution Slope		
	1.1	1.4	1.8
Healthy (Control) Tissue	Stable	Stable	Unstable
Electrophysiology Remodelling Only	Stable	Stable	Stable
Tissue Remodelling Only	Stable	Unstable	Unstable
Electrophysiology + Tissue Remodelling	Stable	Stable	Stable
Deforming Tissue			
	Restitution Slope		
	1.1	1.4	1.8
Healthy (Control) Tissue	Stable	Unstable	Unstable
Electrophysiology Remodelling Only	Stable	Stable	Stable
Tissue Remodelling Only	Stable	Unstable	Unstable
Electrophysiology + Tissue Remodelling	Stable	Stable	Stable

Table 3. Summary of spiral wave stability. Each row represents a combination of static or deforming domain, and whether or not remodelling of electrophysiology and/or tissue (gap junctions, fibrosis) is introduced. The stability in the presence of diffuse fibrosis is assessed on the basis of numerical simulations carried out on mesh F0 of Table 1.

3). The reasons for this may be attributed to the effect that the electrophysiology remodelling has on the restitution slope. It can be seen in Figure 8 that the remodelled electrophysiology produces a much shallower profile for the restitution slope and the more stable configurations have already been seen to be those with lower restitution slopes (see, for example, Figure 2 or [23]).

To simulate tissue fibrosis, gap junction remodelling was introduced by modifying the diffusion tensor and patches of inexcitable tissue were created in the computational mesh. We observed generally that this tissue remodelling can destabilise spiral waves (see, for example, Figure 4), and investigated further the effect of varying the size and density of the patches of fibrotic tissue. The results of these follow-on experiments suggest that reducing the size of the individual regions of inexcitable tissue also weakens the observed destabilising effect (Figure 5). This contrasts with the observations of ten Tusscher and Panfilov [46], whose simulations suggest that diffuse fibrosis stabilises spiral waves supported by the dynamic behaviour of the TP06 model. This might be attributable to the fact that in that work, each fibrotic region was a $0.25 \text{ mm} \times 0.25 \text{ mm}$ square, its dimensions determined by the finite difference mesh they used. Each region is therefore more uniform and approximately one quarter the area of the smallest regions used in our study (Figure 5), where the effects of our remodelling is weakest.

The effect of changing the density of the fibrotic regions for a fixed patch size was less pronounced. In fact, from our numerical simulations it was difficult to determine a consistent pattern and it appears that the size of the fibrotic regions, rather than the percentage of the domain that is inexcitable, is more significant in determining the influence of fibrosis on spiral wave dynamics for the TP06 model.

When the electrophysiology and tissue remodelling is combined with mechanical deformation, the overall effect in our experiments was one of stabilisation (see Figure 7). The stabilising effects of the electrophysiology remodelling dominated the combined destabilising effects of tissue remodelling and mechanical deformation. In fact, as summarised in Table 3, the simulations were always stable whenever the remodelled electrophysiology was used. We suggest that this seemingly contradictory finding may be due to a lack of spatial and/or temporal electrophysiological heterogeneity in the model. Such heterogeneities, which are well known substrates for the initiation of re-entrant arrhythmias [57, 58], may also play a role in the destabilisation of re-entry and cause breakdown of re-entrant waves (*i.e.* degeneration from ventricular tachycardia to fibrillation) [59]. Including such heterogeneities in the model may

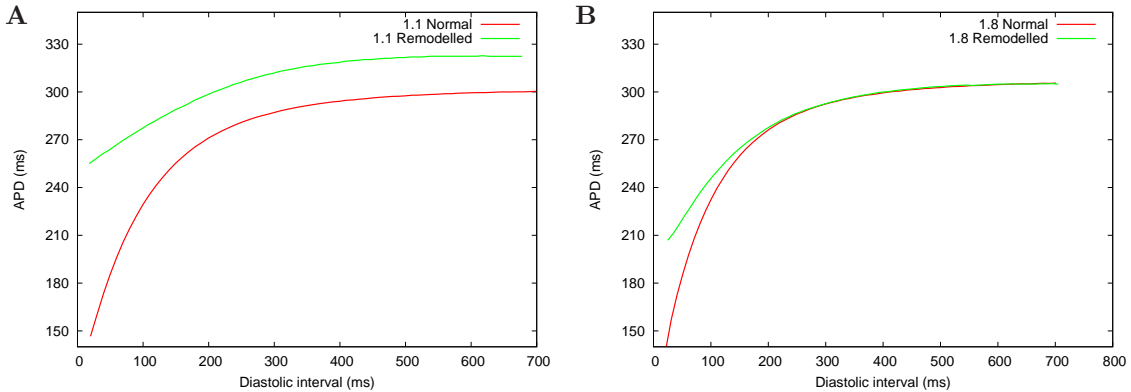


Figure 8. Remodelled restitution slopes. Comparison of restitution slopes for normal and remodelled electrophysiology: (A) 1.1; (B) 1.8.

increase the incidence of spiral wave break-up, despite the stabilising effects of the cellular-level electrophysiological remodelling, and their inclusion is therefore an important next step in model development. Furthermore, although we have included gap junction remodelling in our study, our model does not include a description of the fibre disruption that is commonly seen in heart failure and which has been implicated in arrhythmogenesis (e.g. [60]). Whether or not this particular type of fibre disruption can also result in destabilisation of re-entrant waves remains to be investigated in detail, although it does appear likely [61]. Nevertheless, and despite these two potential areas for further study, our model has highlighted several electromechanical mechanisms that increase or decrease the propensity of ventricular tachycardia to degenerate into ventricular fibrillation.

In this paper, the TP06 model of electrophysiology has been coupled with a Mooney-Rivlin model of mechanical response, and additional assumptions (outlined in the paper) have been made about the remodelling effect that failing tissue has on the dynamics of the system and the model parameters. For this combination of models, we have observed that:

- changes in electrophysiology introduced to simulate failing cardiac tissue can stabilise the electrical dynamics;
- the introduction of inexcitable fibrotic regions can cause a previously stable spiral wave to break up;
- in such cases, the sizes of the individual fibrotic regions seem to have a stronger influence on stability than their overall density – decreasing the size of the fibrotic regions increased stability;
- the stabilisation effects of the remodelled electrophysiology are strong enough to overcome break-up caused by the combined effects of mechanical deformation and fibrosis.

These observations relate to a specific combination of models for simulating coupled electromechanical behaviour, and it would be interesting for future research to investigate whether they are indicative of the effects of diffuse fibrosis on spiral wave stability for a broader range of models. The computational framework presented here is flexible enough to provide the basis for a study of this type, but improvements would need to be made to the efficiency of the underlying numerical algorithms if simulations are to be carried out in three space dimensions with meshes fine enough to resolve the wave-fronts generated by electrophysiology models such as TP06. This is the subject of ongoing research, early results of which

indicate that mesh adaptivity can significantly improve computational efficiency [33]. Furthermore, the replacement of the general-purpose ILU preconditioner with an optimal (multigrid-based) preconditioner would remove the dependence of the convergence of the iterative solver on user-defined parameters. If an efficient, parallel, implementation of these techniques can be developed then the effects of diffuse fibrosis can be explored more thoroughly and, ultimately, three-dimensional simulations of cardiac dynamics in heterogeneous tissue could be carried out on realistic geometries.

Acknowledgments

NRK was supported by an Engineering and Physical Sciences Research Council Doctoral Training Grant. APB was supported by a Medical Research Council Special Training Fellowship in Biomedical Informatics (G0701776).

References

1. American Heart Association (2010) Executive summary: Heart disease and stroke statistics 2010 update: a report from the American Heart Association. *Circulation* 121: 948-954.
2. Tomaselli GF, Zipes DP (2004) What causes sudden death in heart failure? *Circulation Research* 95: 754-763.
3. Jalife J (2000) Ventricular fibrillation: mechanisms of initiation and maintenance. *Annual Review of Physiology* 62: 25-50.
4. Bers DM (2006) Altered cardiac myocyte Ca regulation in heart failure. *Physiology* 21: 380-387.
5. Glukov AV, Fedorov VV, Lou Q, Ravikumar VK, Kalish PW, et al. (2010) Transmural dispersion of repolarization in failing and nonfailing human ventricle. *Circulation Research* 106: 981-991.
6. Riehle C, Wende AR, Zaha VG, Pires KM, Wayment B, et al. (2011) PGC-B deficiency accelerates the transition to heart failure in pressure overload hypertrophy. *Circulation Research* 109: 783-793.
7. Yoshida M, Ohkusa T, Nakashima T, Takanari H, Yano M, et al. (2011) Alterations in adhesion junction precede gap junction remodelling during the development of heart failure in cardiomyopathic hamsters. *Cardiovascular Research* 92: 95-105.
8. Polyakova V, Loeffler I, Hein S, Miyagawa S, Piotrowska I, et al. (2011) Fibrosis in endstage human heart failure: Severe changes in collagen metabolism and MMP/TIMP profiles. *International Journal of Cardiology* 151: 18-33.
9. Noble D (2002) The rise of computational biology. *Nature Reviews Molecular Cell Biology* 3: 460-463.
10. Clayton RH, Bernus O, Cherry EM, Dierckx H, Fenton FH, et al. (2011) Models of cardiac tissue electrophysiology: Progress, challenges and open questions. *Progress in Biophysics and Molecular Biology* 104: 22-48.
11. Efimov IR, Nikolski VP, Slama G (2004) Optical imaging of the heart. *Circulation Research* 95: 21-33.
12. Walton RD, Benoist D, Hyatt CJ, Gilbert SH, White E, et al. (2010) Dual excitation wavelength epifluorescence imaging of transmural electrophysiological properties in intact hearts. *Heart Rhythm* 7: 1843-1849.

13. Benson AP, Al-Owais M, Holden AV (2011) Quantitative prediction of the arrhythmogenic effects of de novo hERG mutations in computational models of human ventricular tissues. *European Biophysics Journal* 40: 627-639.
14. ten Tusscher KHWJ, Hren R, Panfilov AV (2007) Organization of ventricular fibrillation in the human heart. *Circulation Research* 100: e87-e101.
15. Fenton F, Karma A (1998) Vortex dynamics in three-dimensional continuous myocardium with fiber rotation: Filament instability and fibrillation. *Chaos* 8: 20-47.
16. Rodriguez B, Burrage K, Gavaghan D, Grau V, Kohl P, et al. (2010) The systems biology approach to drug development: Application to toxicity assessment of cardiac drugs. *Clinical Pharmacology and Therapeutics* 88: 130-134.
17. Benson AP, Bernus O, Dierckx H, Gilbert SH, Greenwood JP, et al. (2011) Construction and validation of anisotropic and orthotropic ventricular geometries for quantitative predictive cardiac electrophysiology. *Interface Focus* 1: 101-116.
18. Trayanova N (2006) Defibrillation of the heart: insights into mechanisms from modelling studies. *Experimental Physiology* 91: 323-337.
19. Aslanidi OV, Benson AP, Boyett MR, Zhang HG (2009) Mechanisms of defibrillation by standing waves in the bidomain ventricular tissue with voltage applied in an external bath. *Physica D* 238: 984-991.
20. Nash MP, Panfilov AV (2004) Electromechanical model of excitable tissue to study reentrant cardiac arrhythmias. *Progress in Biophysics and Molecular Biology* 85: 501-522.
21. Keldermann RH, Nash MP, Gelderblom H, Wang VY, Panfilov AV (2010) Electromechanical wave-break in a model of the human left ventricle. *American Journal of Physiology - Heart and Circulatory Physiology* 299: H134-H143.
22. Pathmanathan P, Whiteley JP (2009) A numerical method for cardiac mechanoelectric simulations. *Annals of Biomedical Engineering* 37: 860-873.
23. ten Tusscher KHWJ, Panfilov A (2006) Alternans and spiral breakup in a human ventricular tissue model. *American Journal of Physiology - Heart and Circulatory Physiology* 291: H1088-H1100.
24. Pertsov AM, Davidenko JM, Salomonsz R, Baxter WT, Jalife J (1993) Spiral waves of excitation underlie reentrant activity in isolated cardiac muscle. *Circulation Research* 72: 631-650.
25. Keener J, Sneyd J (1998) *Mathematical Physiology*. 1998. New York: Springer-Verlag.
26. Malvern LE (1969) *Introduction to the Mechanics of a Continuous Medium*. Prentice-Hall, Inc.
27. Hunter PJ, McCulloch AD, ter Keurs HE (1998) Modelling the mechanical properties of cardiac muscle. *Progress in Biophysics and Molecular Biology* 69: 289-331.
28. Nash MP, Hunter PJ (2000) Computational mechanics of the heart. *Journal of Elasticity* 61: 113-141.
29. Mooney M (1940) A theory of large elastic deformation. *Journal of Applied Physics* 11(9): 582-592.
30. Rivlin RS (1948) Large elastic deformations of isotropic materials. IV. Further developments of the general theory. *Philosophical Transactions of the Royal Society A* 241(835): 379-397.

31. Smaill B, Hunter P (1991) Structure and function of the diastolic heart: material properties of passive myocardium, in *Theory of Heart: Biomechanics, Biophysics, and Nonlinear Dynamics of Cardiac Function*. Springer, pp. 1-29 pp.
32. Whiteley JP, Bishop MJ, Gavaghan DJ (2007) Soft tissue modelling of cardiac fibres for use in coupled mechano-electric simulations. *Bulletin of Mathematical Biology* 69: 2199-2225.
33. Kirk NR (2012) An adaptive, preconditioned, electromechanical model for the simulation of cardiac arrhythmias. Ph.D. thesis, School of Computing, University of Leeds.
34. Kaab S, Dixon J, Duc J (1998) Molecular basis of transient outward potassium current downregulation in human heart failure. *Circulation* 98: 1383-1393.
35. Beuckelmann DJ, Nabauer M, Erdmann R (1993) Alterations of K^+ current in isolated human ventricle myocytes from patients with terminal heart failure. *Circulation Research* 73: 379-385.
36. Schwinger R, Bundgaard H, Mller-Ehmsen J, Kjeldsen K (2003) The Na, K-ATPase in the failing human heart. *Cardiovascular Research* 57: 913-920.
37. Hasenfuss G, Wolfgang S, Lehnart SE, Preuss M, Pieske B, et al. (1999) Relationship between Na^+Ca^{2+} exchanger protein levels and diastolic function of failing human myocardium. *Circulation* 99: 641-648.
38. Jiang MT, Lokuta AJ, Farrell EF, Wolff MR, Haworth RA, et al. (2002) Abnormal Ca^{2+} release, but normal ryanodine receptors, in canine and human heart failure. *Circulation Research* 91: 1015-1022.
39. Dash R, Frank KF, Carr AN (2001) Gender influences on sarcoplasmic reticulum Ca^{2+} handling in failing human myocardium. *Journal of Molecular and Cellular Cardiology* 33: 1345-1353.
40. Ai AIX, Pogwizd SM (2005) Connexin 43 downregulation and dephosphorylation in nonischemic heart failure is associated with enhanced colocalized protein phosphatase type 2a. *Circulation Research* 96: 54-63.
41. Dupont E, Matsushita T, Kaba RA, Vozi C, Coppens SR, et al. (2001) Altered connexin expression in human congestive heart failure. *Journal of Molecular and Cellular Cardiology* 33(2): 359-371.
42. Jongsma HJ, Wilders R (2000) Gap junctions in cardiovascular disease. *Circulation Research* 86: 1193-1197.
43. Thomas SP, Kucera JP, Bircher-Lehmann L, Rudy Y, Saffitz JE, et al. (2003) Impulse propagation in synthetic strands of neonatal cardiac myocytes with genetically reduced levels of Connexin43. *Circulation Research* 92: 1209-1216.
44. Everett TH, Olgin JE (2007) Atrial fibrosis and the mechanisms of atrial fibrillation. *Heart Rhythm* 4(3 Suppl): S24-S27.
45. Assomull RG, Prasad SK, Burman E, Khan M, Sheppard M, et al. (2006) Cardiovascular magnetic resonance, fibrosis and prognosis in dilated cardiomyopathy. *Journal of the American College of Cardiology* 48: 1977-1985.
46. ten Tusscher KHWJ, Panfilov AV (2007) Influence of diffuse fibrosis on wave propagation in human ventricular tissue. *Europace* 9: vi38-vi45.
47. Spach M, Heidlage JF, Dolber P (2007) Mechanism of origin of conduction disturbances in aging human atrial bundles: Experimental and model study. *Heart Rhythm* 4: 175-185.

48. Rossi MA (2001) Connective tissue skeleton in the normal left ventricle and in hypertensive left ventricular hypertrophy and chronic chagasic myocarditis. *Medical Science Monitor* 7(4): 820-832.
49. Gresho PM, Sani RL (2000) *Incompressible Flow and the Finite Element Method, Volume 2, Isothermal Laminar Flow*. Wiley.
50. Thomas JW (1995) *Numerical Partial Differential Equations: Finite Difference Methods*. Texts in Applied Mathematics. New York: Springer-Verlag.
51. Saad Y, Schultz MH (1986) GMRES: A generalized minimal residual algorithm for solving non-symmetric linear systems. *SIAM Journal on Scientific and Statistical Computing* 7: 856-869.
52. Kelley CT (1987) *Iterative Methods for Linear and Nonlinear Equations*. Society for Industrial Mathematics.
53. Saad Y (1996) *Iterative Methods for Sparse Linear Systems*. PWS Publishing Company.
54. Chen K (2005) *Matrix preconditioning techniques and applications*. Cambridge University Press.
55. ten Tusscher KHWJ, Noble D, Noble PJ, Panfilov AV (2004) A model for human ventricular tissue. *American Journal of Physiology - Heart and Circulatory Physiology* 286: H1573-H1589.
56. Kirk NR, Benson AP, Goodyer CE, Hubbard ME (2011) Application of an efficient coupled electromechanical solver to investigate end stage human heart failure. *Computing in Cardiology* 2011 38: 17-20.
57. Tomaselli GF, Marban E (1999) Electrophysiological remodeling in hypertrophy and heart failure. *Cardiovascular Research* 42: 270-283.
58. Lou Q, Janks DL, Holzem KM, Lang D, Onal B, et al. (2012) Right ventricular arrhythmogenesis in failing human heart: The role of conduction and repolarization remodeling. *American Journal of Physiology - Heart and Circulatory Physiology* 303: H1426-H1434.
59. Keldermann RH, ten Tusscher KHWJ, Nash MP, Hren R, Taggart P, et al. (2008) Effect of heterogeneous APD restitution on VF organization in a model of the human ventricles. *American Journal of Physiology - Heart and Circulatory Physiology* 294: H764-H774.
60. Benoist D, Stones R, Drinkhull MJ, Benson AP, Yang Z, et al. (2012) Cardiac arrhythmia mechanisms in rats with heart failure induced by pulmonary hypertension. *American Journal of Physiology - Heart and Circulatory Physiology* 302: H2381-H2395.
61. Benson AP, Benoist D, Gilbert SH, Holden AV, Stones R, et al. (2011) Structural and functional remodelling both contribute to arrhythmia substrate in computational models of right heart failure. *Proceedings of The Physiological Society* 23: PC129.